Journal of
Materials Chemistry A

Colloidal Three-Dimensional Covalent Organic Frameworks and Their Application as Porous Liquids

Journal:	*Journal of Materials Chemistry A*
Manuscript ID	TA-ART-07-2020-006768.R1
Article Type:	Paper
Date Submitted by the Author:	13-Oct-2020
Complete List of Authors:	Mow, Rachel; National Renewable Energy Laboratory Lipton, Andrew; Pacific Northwest National Laboratory Shulda, Sarah; National Renewable Energy Laboratory Gaulding, Ashley; National Renewable Energy Laboratory, Gennett, Thomas; NREL, Braunecker, Wade; National Renewable Energy Laboratory,

Journal Name

ARTICLE TYPE

Cite this: DOI: 00.0000/xxxxxxxxxx

Colloidal Three-Dimensional Covalent Organic Frameworks and Their Application as Porous Liquids[†]

Rachel E. Mow,[ab] Andrew S. Lipton,[c] Sarah Shulda,[b] E. Ashley Gaulding,[b] Thomas Gennett,[*ab] and Wade A. Braunecker[*ab]

Received Date
Accepted Date

DOI: 00.0000/xxxxxxxxxx

Developing solid porous materials into free-flowing liquids with permanent porosity is a promising strategy for overcoming certain limitations of conventional sorbent materials employed in gas storage and separation applications. The ability to control the pore size and chemical functionalities of organic frameworks gives these particular nanoporous materials distinct advantages over other small cage-like molecules or hollow particles that have been developed into porous liquids. Here, we describe the synthesis of a 3D imine-linked colloidal covalent organic framework (COF)-based porous liquid, designed for efficient size-exclusion of solvent, as well as for long-term stability. By tethering ionic liquids to the colloid surface, the colloids can be dried, purified, and resuspended in a variety of solvents without irreversible aggregation typically observed of COF colloids. Colloid size could be controlled between 50 and 400 nm, with surface areas as high as 800 m^2/g. The 3D intertwining morphology of the colloids had pore sizes ranging from 5 to 14 Å, allowing them to efficiently size-exclude bulky ionic liquids. The COF colloids were stable towards flocculation in an ionic liquid for > 1 year. Permanent porosity was confirmed with a combination of ^{19}F NMR measurements and gas sorption techniques. CO_2 and CH_4 uptake in these porous liquids increased more than 10 and 20-fold, respectively, over non-porous, neat ionic liquid control samples. The work not only advances the state of COF-based colloid science but also represents a practical advance towards developing more robust, tunable framework-based porous liquid materials for a host of gas storage and separation applications.

1. Introduction

Porous liquids were introduced as a theoretical concept in 2007 as materials that could maintain permanent porosity while also having the property of fluidity.[1] However, their synthesis proved non-trivial, and the materials essentially remained hypothetical until 2014 with the discovery that small imine-based organic cages could be made liquid near room temperature through judicious functionalization. With dramatically increased gas sorption capacities and diffusion rates over non-porous liquid control samples, the materials have become exciting prospects for a range of gas separation and storage applications. Porous liquids have since been realized with several additional unique strategies, including functionalizing hollow silica spheres with liquid polymers,[2] dissolving small organic porous cages in sterically excluded solvents like crown ether,[3,4] and suspending zeolites or metal organic frameworks (MOFs) in bulky size-excluded solvents.[5–9] The latter class of materials are particularly attractive given the well-developed field of solid-state MOFs for gas storage and separation applications and all of the knowledge regarding their highly tunable pore environments that would be transferable to the field of porous liquids.

Despite these advantages, MOF-based porous liquids have some drawbacks. For instance, the flexible nature of many MOF structures renders them subject to pore collapse in the presence of moisture when undergoing a pressure swing.[10] As these are the very conditions required for industrial carbon capture and other gas purification applications,[11,12] for which many porous liquid materials were purportedly developed, more robust materials are needed to advance the field. Similar to MOFs, covalent organic frameworks (COFs) are high surface area materials with periodic structures and highly tunable pore environments, but COFs are composed entirely of light elements and are connected by much more rigid, covalent bonds.[13,14] They have recently been

---

[*] Co-corresponding authors

[a] *Department of Chemistry, Colorado School of Mines, Golden, CO 80401, United States. Fax: 303-273 3629; Tel: 303-273 3610*

[b] *National Renewable Energy Laboratory, Golden, CO 80401, United States. Tel: 303-275-3000*

[c] *Environmental Molecular Sciences Laboratory, Pacific Northwest National Laboratory, Richland, Washington 99354, United States*

[†] Electronic Supplementary Information (ESI) available: Synthetic schemes, NMR spectra, DRIFTS spectra, porosity characterization, particle size distributions, XRD patterns, isotherms. See DOI: 00.0000/00000000.

employed for a range of applications, including gas storage and separation,[15–17] drug delivery,[18–20], energy storage,[21] and as supports for catalysts.[22–25] Many COFs, particularly imine-based frameworks, are considerably more stable than most MOFs; in fact, certain imine-based COFs retain their crystallinity and surface area under extremely aggressive conditions (3 M HCl, 20 M NaOH, or boiling water for > 1 month).[26]

In addition to structural and chemical stability, the long-term stability of framework-based porous liquid suspensions towards aggregation/flocculation is another important consideration for any potential continuous flow application, where flocculation would otherwise cause reactor fouling. While numerous techniques have been developed to synthesize stable colloidal MOF suspensions in a variety of solvents,[27–35] the state of colloidal COF science is much less developed. Dichtel, et. al., recently developed a successful technique for generating stable colloidal COF suspensions of particles ranging from 200 – 600 nm using nitrile-based solvents.[36–38] COF colloids have since been developed with this technique for a variety of applications ranging from thin film development[36,39] to single crystal formation,[40,41] nanoparticle encapsulation,[42] and sensors within biological specimens.[43] We contend colloidal COFs would also have great potential benefit in the field of porous liquids. However, using current state-of-the-art techniques, COF colloids generally cannot be removed from the nitrile solvent without the unintended consequence of inducing irreversible aggregation, which in our experience, causes them to float in ionic liquids (*vide infra*).

This work advances the state of framework-based colloid science and the field of porous liquids through the development of (1) the first reported method to synthesize a high surface area, small pore 3D-imine based colloidal framework suspension, (2) a technique for functionalizing the 'shell' of colloidal COFs so that they can be dried, purified, and resuspended in a variety of non-nitrile based solvents, and (3) the application of the first stable colloidal COF-based porous liquid with enhanced CO_2 and CH_4 uptake over non-porous control liquids.

2. Results/Discussion

2.1. COF Colloid Synthesis

To facilitate the formation of a stable COF-based porous liquid, we targeted the development of COF particles with both sub 1 nm pores (to size-exclude solvent) and small particle sizes (to help make indefinite suspension possible). We chose to investigate imine-based COFs because they are considerably more robust than boron-based COFs. COFs can be synthesized as 2D or 3D materials, based on the dimensionality of the linking unit. 2D COFs are synthesized from planar building blocks, forming sheets that π-stack to create porous channels. There have been several reports of controlled colloidal growth of 2D-imine COFs that inspired this work, but 2D COFs typically have large pore diameters (>2 nm), much too large to size-exclude most solvent molecules for porous liquid applications. Post-synthetic functionalization strategies can be used to tether functionalities to the COF walls that effectively reduce the pore size closer to 1 nm, but these strategies typically disrupt packing, resulting in lower effective surface areas.[21]

3D COFs are typically synthesized from tetrahedral building blocks. The advantage of these materials for porous liquids are their smaller effective pore sizes, which form as a result of intertwining/interpenetration of the network-like morphology. In two recent literature surveys of a combined approximately 190 imine COFs, a screen of materials with surface areas > 500 m^2/g and pore widths < 1.4 nm revealed thirty six 3D COFs and only one known 2D COF with these characteristics.[44,45] Indeed, the effective pore-size of COF-300 (Fig. 1A, illustrated as a non-interpenetrating structure for clarity) was originally reported as 8 Å.[46] However, the porosity of COF-300 is highly dependent on synthetic conditions and has been reported as high as 14 Å.[47] We hypothesized this COF could make an effective porous liquid with a sterically excluded room temperature ionic liquid based on the bulky tetrakis(3,5-bis(trifluoromethyl)phenyl) borate) anion (so-called BAr^F anion) that has a diameter between 13 and 14 Å (Fig. 1B). Furthermore, since thirty five other 3D imine COFs have similar or smaller pore sizes,[45] we believe this COF to be representative of the potential of this class of materials to form porous liquids.

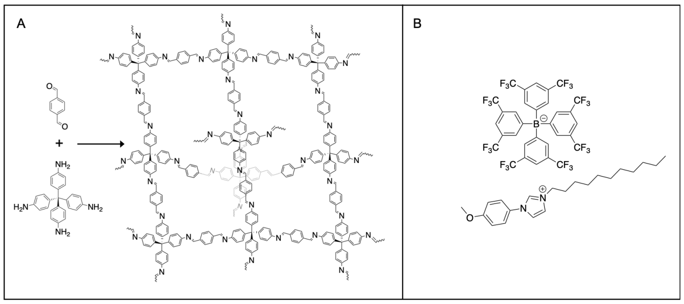

Fig. 1 a) Synthesis and chemical structure of the repeat unit of COF-300, illustrated as a non-interpenetrating structure for clarity. b) The bulky, size-excluded BAr^F ionic liquid used to suspend COF-300 in this work to create a porous liquid.

Original literature conditions for the synthesis of colloidal 2D imine-linked COFs employed $Sc(OTf)_3$ as a potent Lewis acid catalyst for room temperature synthesis in dilute acetonitrile solvent.[37] Using these same solvent/catalyst conditions, we synthesized 3D imine-linked COF-300 colloids with excellent control over particle size (between 50 and 250 nm, Fig. S3, particle size being commensurate with monomer concentration). Characterization of the IR stretching frequencies of the COF product (*e.g.*, imine C=N stretching at 1624 cm^{-1} and C-C=N-C stretching at 1202 cm^{-1}, Fig. S21) are fully consistent with those reported in the literature for COF-300.[46]

However, these colloids were amorphous (as determined by XRD) with surface areas between 20 and 200 m^2/g. It has been well established that the formation of high surface area, crystalline imine-linked COFs occurs first through the formation of amorphous intermediates.[47] The application of longer reaction times, hotter temperatures, and co-solvents (such as moisture) that promote imine bond reversibility often results in defect correction and improved COF crystallinity. We made several attempts to improve the surface area of colloidal COF-300 by tweaking reaction conditions. Unfortunately, longer reaction times (> 5 days) result in larger particles that eventually flocculate from solution, and the use of other solvents (benzonitrile, chlorobenzene, DMSO, and moisture) resulted in non-colloidal heterogenous mixtures, even at very dilute monomer concentrations. Higher temperatures (90°C) did improve surface area to near 400 m^2/g, but the catalyst appeared unstable under these conditions at higher temperatures (120°C), as evidenced by the formation of a substantial amount of black precipitate during the reaction. However, by using a trifluoroacetic acid catalyst, we achieved COF-300 colloids with surface area of 600 m^2/g synthesized at 120°C over 72 hours (summary of most pertinent results in Table S1). These conditions were further extended to a methoxy-functionalized COF (monomers illustrated in Fig. S2) to achieve 3D-colloidal COF particles with a surface area near 800 m^2/g (Fig. S16).

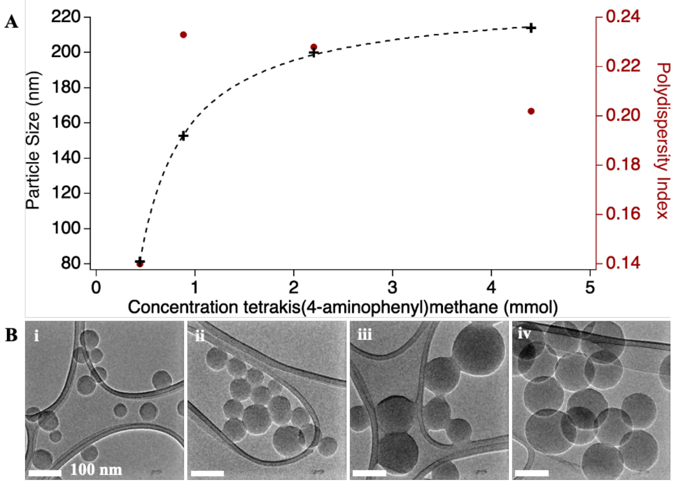

Fig. 2 a) Dynamic light scattering data for batches of colloidal COF-300 with varying concentration of the tetrakis(4-aminophenyl)methane monomer, and b) TEM images of colloidal COF particles synthesized with i) 0.44 mM, ii) 0.88 mM, iii) 2.2 mM and iv) 4.4 mM tetrakis(4-aminophenyl)methane in acetonitrile.

Dynamic light scattering data suggests we can control COF particle sizes by varying the monomer concentration in acetonitrile (results summarized in Fig. 2A), with average particle sizes ranging from 80 nm to 215 nm based on the concentration of tetrakis(4-aminophenyl)methane in acetonitrile (peak distribution shown in Fig S8). The COF particle sizes were further confirmed by transmission electron microscopy (TEM), shown in Fig. 2B. While the smaller particles synthesized under more dilute conditions were not entirely uniform in size, they are all spherical in nature. Dispersity improved for the larger (215 nm) particles. X-ray diffraction on the COF colloids revealed a semi-crystalline material, though the diffraction peaks were quite broad (Fig. S10).

Solvent exchange is typically used to purify COFs, but the COF colloids irreversibly aggregate in solvents other than acetonitrile. However, we discovered that the colloids could be resuspended following centrifugation, so long as they were never fully removed from acetonitrile. After centrifugation at 14,000 rpm for 10 minutes, the acetonitrile supernatant containing excess unreacted monomers and catalyst was decanted from the loosely packed colloids. The colloids were then resuspended in fresh acetonitrile through 5 minutes of sonication. This process was repeated five times to purify the COF colloids. DLS revealed that the colloid size did not appreciably change during this purification process (Fig. S9).

2.2. Functionalization of Colloids

Next, we developed a strategy to functionalize the outer shell of the COF to improve colloid stability. Pendant, unreacted amine and aldehyde groups at the surface of the colloid can react with each other when the colloids are in close proximity, effectively causing them to cross-link. In our experience, this happens slowly in solution over the course of days/weeks (as suggested by DLS), or immediately when the colloids are precipitated/dried. In our approach, we functionalized the COF shell by reacting pendant amine groups at the surface with an aldehyde functionalized imidazolium BAr^F-based salt shown in Scheme 1 (synthesis illustrated in Scheme S1 of the SI). We designed this compound so that it would be size-excluded from the interior of the COF and would only react at the surface. A large molar excess of aldehyde functionalized salt was dissolved in acetonitrile and injected into a purified colloidal suspension along with fresh catalyst, and the reaction was stirred at 90 °C for 24 hours. Following a similar centrifugation workup as described above to purify the functionalized colloids, remarkably, the COF colloid could now be fully dried under vacuum and then resuspended in acetonitrile (Fig. S4) as a colloidal solution. DLS revealed the average particle size doubled during this functionalization reaction, likely from a combination of the added tethered BAr^F layer as well as some irreversible particle aggregation during the functionalization and workup (Fig. S9).

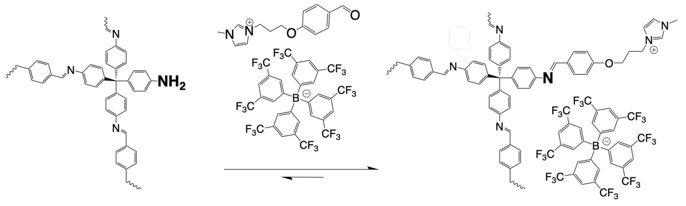

Scheme 1 Functionalization of the pendent, unreacted amines at the surface of a COF-300 particle with an aldehyde functionalized BAr^F-based ionic liquid compound.

Diffuse reflectance infrared Fourier transform spectroscopy (DRIFTS) of the functionalized colloids confirmed the presence of new stretches at 1150 cm^{-1} and 680 cm^{-1}, attributed to C-F and imidazolium functionalities, respectively, from the tethered BAr^F compound (Figs. S20 and S21). Nitrogen adsorption showed the surface area after functionalization decreased from 600 to 433 m^2/g. This slight reduction in surface area and the loss of the 12 Å and 14 Å peaks in the pore size distribution suggests that the large excess of aldehyde functionalized BArF salt used in the synthesis may have partially clogged some of the larger pores, but left the smaller pores open (Figs. S18 and S19). Regardless, the work represents a successful advance in post-synthetic modifications of

COF colloids. The colloids can now be resuspended in a variety of solvents (including nitrile solvents as well as acetone, methanol, and dichloromethane), which was not previously possible, as observed in the literature and observed by us with extensive control experiments.

2.3. Stability of Colloidal COF-300 Suspensions in BAr^F Ionic Liquid

Porous liquids were made by suspending the purified COF particles in a BAr^F-based room temperature ionic liquid (Fig. 1B), which undergoes a glass transition at -20 °C.[48] The first suspension was made from uncontrolled, micron sized COF particles, synthesized using the procedure developed by Uribe-Romo et al.[46] Slight visible separation of the particles from the mixture could be observed at the end of one week, but the ionic liquid is fairly viscous at room temperature and separation is expected to be slow under these conditions. We accelerated separation by centrifuging the porous liquid at 6000 rpm for 3 h, at which point it was clear the COF particles floated to the top of the mixture (Fig. S5).

Purified colloids 200 nm in diameter (non-functionalized shell) were suspended in acetonitrile and mixed with BArF ionic liquid. The acetonitrile was removed on a rotorary evaporator, and the porous liquid was dried in vacuo at 80 °C while stirring overnight to remove all traces of volatile solvent. No separation of the COF colloids from the ionic liquid was observed after 5 hours of centrifugation at 6,000 rpm (Fig. S6). A 2 wt.% suspension of colloidal COF in ionic liquid has been stable towards any visible separation for > 1 year. While these non-functionalized colloids appear stable towards separation/flotation in the ionic liquid, they cannot be resuspended in acetonitrile as a colloidal solution once introduced into the ionic liquid, suggesting some irreversible aggregation/cross-linking does still occur. However, the BAr^F-functionalized colloids are more robust, with aggregation in the ionic liquid appearing to be minimal. Porous liquids were made with increased colloidal COF-loading, up to 30 wt.% COF in the BAr^F ionic liquid. At loadings greater than 30 wt.% the viscosity was such that a stir bar could not stir the mixture at temperatures less than 100 °C.

We also suspended the 8 Å pore COF-300 in an IL based on a bistriflimide anion and bulky diazabicycloundecene (DBU) cation (7.7 Å diameter).[49] The relative COF pore size and IL size suggested this system was on the cusp of forming an effective size-excluded porous liquid. However, while we observed COF-300 particles to float with time in the BArF IL (*vide supra*), a 10 wt.% suspension of COF-300 in the bistriflimide IL solidified over the course of a few days, even appearing to 'crack', as the IL was sucked up by the COF. We are currently investigating the ability of our colloidal COF to size exclude a range of other common bulky ionic liquids, including tetraalkylammonium and tetraalkylphosphonium ILs, as well as branched and star-shaped liquid polymers.[6]

2.4. Porosity of Porous Liquids

^{19}F magic angle spinning (MAS) nuclear magnetic resonance (NMR) was used to probe whether the BAr^F anion could penetrate the COF pores. Because adsorbtion of the BAr^F anion into the COF pore would alter its molecular motion, in principle differences in -CF$_3$ dipolar couplings, chemical shift, and the temperature at which chemical shift anisotropy (CSA) is observed would all be influenced such that adsorbed BAr^F could be distinguished from the bulk ionic liquid. 10 wt.% suspensions of two different COFs were prepared in the ionic liquid: COF-300 (with a pore diameter of 14 Å), and a larger pore 2D COF (pore diameter 37 Å, structure illustrated in Fig. S1). The latter was not anticipated to be able to size-exclude the ionic liquid like the former. ^{19}F spectra were measured at -15 °C, where the frozen samples were anisotropic (Fig. 3), and at 0 °C, where the ionic liquid is quite viscous but fluid (Fig. S13).

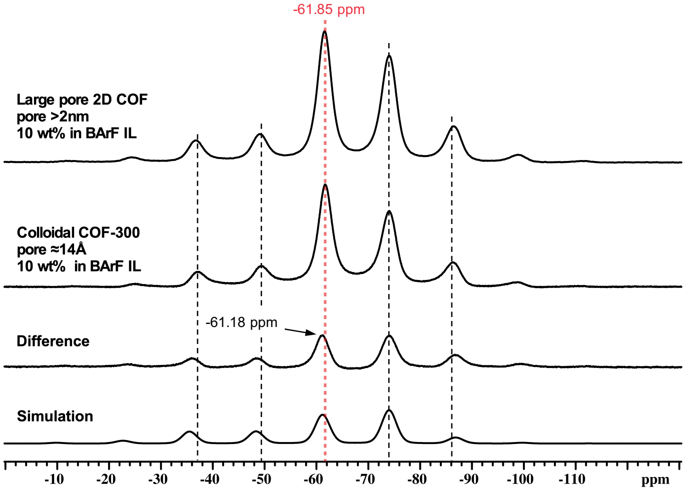

Fig. 3 Solid state ^{19}F MAS NMR spectra of 10 wt.% porous liquid suspensions acquired at -15°C. The difference of these two mass normalized spectra reveals the presence of a small fraction of BAr^F anion in the large pore COF with different dipolar coupling and altered ^{19}F MAS lineshape consistent with reduced mobility. The dashed red line is centered on the isotropic peak of the colloidal COF-300 spectrum, while the dashed black lines are intended as visual queues.

At -15 °C, the line shape of the ^{19}F spectra reflects that of a CSA pattern typically observed for rotating CF$_3$ groups,[50] and the rotationally averaged ^{19}F-^{19}F dipolar coupling[51] and the isotropic chemical shift centered near -62 ppm are also consistent with literature values for comparable compounds.[51–53] Neat BAr^F was frozen and static ^{19}F NMR acquired to verify the presence of the dipolar coupling. At first glance, there appears to be little difference between the spectra of the COF-300 suspension and the large pore 2D COF at this temperature. However, by taking the difference of these two mass normalized spectra, the spectrum of the free/bulk ionic liquid can effectively be removed. The results suggest the 2D COF sample contains a small fraction of BAr^F anion not present in the smaller pore 3D COF sample that has a different dipolar coupling and altered ^{19}F MAS lineshape, suggesting this species has further reduced mobility.[52]

At 0 °C, differences in the spectra are much more pronounced. The small pore COF-300 suspension exhibited a single sharp, symmetric peak near -62 ppm, as would be anticipated for an isotropic spectrum if all fluorine atoms were in a homogenous environment. In contrast, the ^{19}F spectrum of the BAr^F anion in the 2D COF suspension revealed a significantly broader resonance at -62 ppm (line width more broad by a factor of about 3), and a second smaller, broad peak near -74 ppm, consistent with the peak observed in the anisotropic spectrum at -15 °C. Qualitatively, the broad peaks suggest there could be exchange of the BArF anion between different environments at this temperature, but the simple fact that a small fraction of the BArF anion in the large pore suspension displays partial anisotropic behavior while the COF-300 suspension is isotropic at 0 °C strongly suggests COF-300 efficiently excludes the BArF anion.

CO_2 adsorption measurements were performed to further investigate porosity in the COF-300 suspension and to probe how adsorption of CO_2 is enhanced over the neat ionic liquid. The isotherms were measured at 0 °C with a ten-minute equilibration time between data points. Fig. 4 shows the isotherms for the solid-state COF-300, the neat BAr^F ionic liquid, and a porous liquid with approximately 20 wt.% COF loading. Over the entire range of relative pressures investigated at 0 °C, CO_2 uptake for the 20 wt.% porous liquid was intermediate between the neat ionic liquid and the solid state COF.

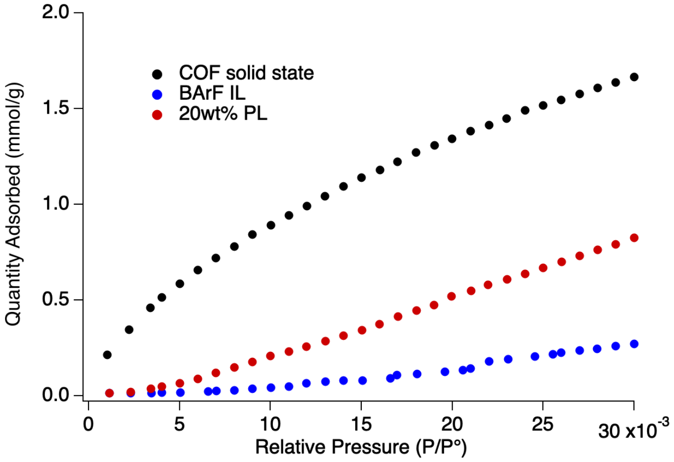

Fig. 4 CO_2 adsorption isotherms at 0°C on the solid-state COF, neat BAr^F ionic liquid, and 20wt% porous liquid (PL). The quantity of CO_2 adsorbed was normalized to the total mass of the sample.

2.5. Temperature Programmed Desorption

CO_2 and CH_4 temperature programmed desorption (TPD) measurements were done on the porous liquids for a quantitative assessment of the gas uptake. The samples were dosed with an overpressure of 1.5 atm of the respective gas at 70 °C, and then the sample was quenched with an ethanol/liquid N_2 bath (-115 °C) for the CH_4 measurements or an ethanol/dry ice bath (-78 °C) for the CO_2 measurements. The quench froze the sample, allowing the head space to be pumped free of excess gas. The sample temperature was then ramped at 15 °C min^{-1} while held under vacuum. The TPD was coupled with a mass spectrometer that monitored gas evolution. The output signal from the mass spectrometer was divided by the mass of the sample to create a mass normalized signal that was integrated over the full temperature range to determine total quantity of gas desorbed.

Fig. 5 shows the CO_2 and CH_4 TPD traces for the solid-state COF-300, the neat BAr^F ionic liquid, the 20 wt.% porous liquid, and the 30wt% porous liquid. The 20 wt.% porous liquid took up 7.6x more CO_2 and 12x more CH_4 than the neat ionic liquid. The 30 wt.% porous liquid adsorbed 1.5x more CO_2 and 1.8x more CH_4 than the 20 wt.% porous liquid, indicating that gas uptake roughly scales proportionately with the weight fraction of COF in the porous liquid.

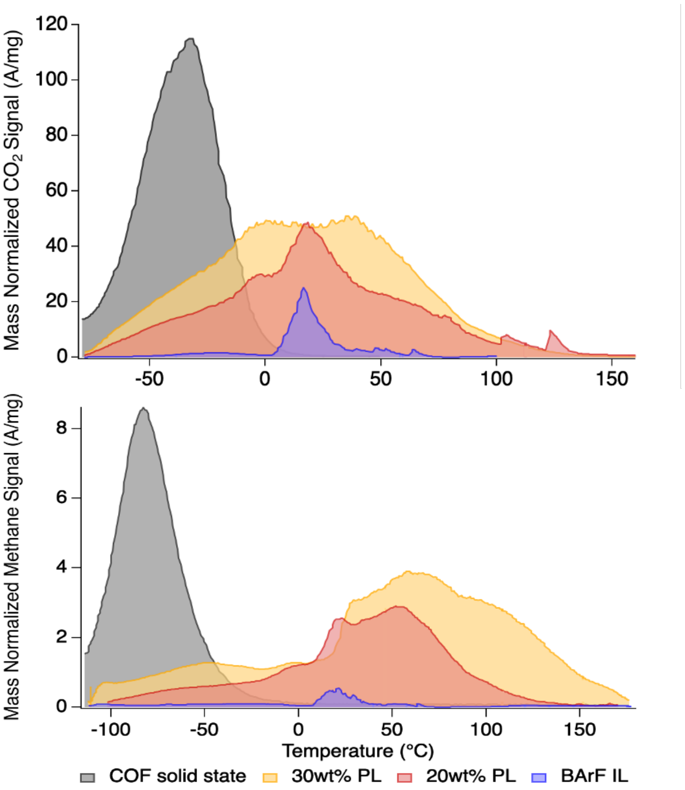

Fig. 5 a) CO_2 and b) CH_4 TPD on the solid state COF-300 (black), neat BAr^F ionic liquid (blue), the 20 wt.% porous liquid (red), and the 30 wt.% porous liquid (yellow).

It is worth noting that under the conditions of the TPD experiment (15 °C min^{-1} ramp rate), neither CO_2 nor CH_4 start to significantly desorb from the neat ionic liquid until it is heated above 0 °C, or just above its glass transition temperature, with peak desorption of both gasses occurring near room temperature. Thus, the neat frozen ionic liquid appears fairly effective at trapping dissolved gas. For the solid-state COF, CO_2 desorption peaked at -33 °C and CH_4 at -83 °C. For the 20 wt.% porous liquid, desorption behavior is intermediate between the neat ionic liquid and the solid state COF. For example, peak desorption temperatures resemble that of the neat ionic liquid, suggesting the frozen ionic liquid may assist in trapping gas in the COF pores. However, a fraction of the gas does 'leach' from the frozen porous liquid even at cryogenic temperatures. We are currently investigating the efficacy of using other glassy and crystalline matrices to effectively control gas desorption behavior, an important consideration for numerous gas storage technologies, by tuning the melt or glass transition temperatures of the porous liquid matrix.

3. Conclusions

This work advances the state of framework-based colloid science by reporting for the first time a synthetic technique for capping and stabilizing COF colloids, thereby allowing them to be dried, resuspended, and utilized in a variety of solvents without irreversibly aggregating. These robust materials were then used to develop the first colloidal COF-based porous liquids, stable towards flocculation on the benchtop for > 1 year. Permanent porosity in these liquid materials was confirmed with a combination of ^{19}F NMR measurements and gas sorption techniques. CO_2 and CH_4 uptake in these porous liquids increased more than 10 and 20-fold, respectively, over non-porous, neat ionic liquid control samples, and preliminary results indicate that the glass transition and/or melting temperatures of the liquid matrix may be an effective tool for influencing gas desorption temperatures from the porous liquid. This work sets the stage for the development of more robust framework-based porous liquid materials for gas storage and separation applications. We are currently tailoring materials to specifically withstand acidic impurities encountered in certain gas separation applications and are performing reliability studies on rigid materials designed to maintain their structural integrity under the high shear strains encountered under continuous flow conditions.

4. Experimental

4.1. Materials and Synthesis

General. The tetrakis(4-aminophenyl)methane monomer was purchased from TCI America, sodium tetrakis[3,5-bis(trifluoromethyl)phenyl)borate] (Na BAr^F) was purchased from 1Click Chemistry, and all remaining chemicals and precurosors were purchased from Aldrich. Column chromatography was performed with Fluka Silica Gel 60 (220 - 440 mesh). Acetonitrile (and any other solvents attempted for colloidal COF syntheses) was thoroughly dried over 3Å molecular sieves and then passed through a 0.45 micron PTFE filter prior to use. Heavy walled glass pressure vessels with PTFE caps were used in the syntheses of all COF materials. 3-decyl-1-(4-methoxyphenyl)-1H-imidazol-3-ium BAr^F ionic liquid was synthesized according to literature procedure.[48]

Synthesis of 3-(3-(4-formylphenoxy)propyl)-1-methyl-1H-imidazol-3-ium. The overall reaction is summarized in Scheme S1. 4.18 g of 1-methylimidazole (51 mmol) and 10.114 g of 4-(2-chloroethoxy)benzaldehyde (55 mmol) were dissolved in 85 mL dry acetonitrile and reacted at 100°C for 48 hours.[48] The reaction was cooled to room temperature, and the solvent was removed with a rotary evaporator. The solid material was dissolved in DI water and washed with ethyl acetate three times. The product was dried under vacuum at 100°C and used without further purification. 3.0684 g (3.5 mmol) of Na BAr^F was dissolved in 40 mL chloroform and stirred at 50°C for 1 hour to dissolve. The imidazolium chloride intermediate was dissolved in 30 mL chloroform and then mixed with the Na BAr^F solution. The reaction was stirred at 40°C for 24 h, during which time NaCl precipitated from solution. NaCl was filtered from the solution, and the product was purified with flash chomotagraphy in dichloromethane. The compound was characterized with ^{1}H NMR, ^{13}C NMR, and FTIR (see Supporting Information), and peaks are consistent with those of literature analogues.[54] ^{1}H NMR (400 MHz, DMSO-d$_6$): δ 9.87 (s, 1H), 9.15 (s, 1H), 7.85 (d, 2H, J = 9.2 Hz), 7.81 (s, 1H), 7.71 (s, 1H), 7.66 (s, 4H), 7.62 (s, 8H), 7.08 (d, 2H, J = 8.8 Hz), 4.37 (t, 2H, J = 7.0 Hz), 4.16 (t, 2H, J = 5.8 Hz), 3.85 (s, 3H), 2.32 (m, 2H). ^{13}C NMR (100 MHz, DMSO-d$_6$): δ 191.2, 163.1, 161.7, 161.2, 160.7, 160.2, 136.8, 134.0, 131.7, 129.8, 128.6, 128.3, 128.0, 125.3, 123.6, 122.6, 122.4, 117.5, 114.8, 65.1, 46.3, 35.7, 28.8.

COF synthesis. COF-300 with uncontrolled particle size was synthesized according to a literature procedure.[46] The particles were collected with a 10 μM filter, and after drying, the surface area was recorded as 730 m^2/g. Similarly, the large pore 2D COF (Fig. S1) was synthesized according to literature procedure.[55] The surface area for the sample used in the NMR study was 550 m^2/g.

Colloidal COF synthesis. Colloidal COFs were synthesized by dissolving 80.6 mg (0.21 mmol) of tetrakis(4-aminophenyl)methane and 59.3 mg (0.44 mmol) of terephthaldehyde in 40 mL dry acetonitrile. The solution was sparged with nitrogen. 10 μL of trifluoroacetic acid or 50 mg (0.1 mmol) of Sc(OTf)$_3$ dissolved in 10 mL of dry acetonitrile and sparged with nitrogen, was added to the monomer solution. The reaction was stirred at the desired temperature for 72 h, after which time it was cooled to 60°C and was hot filtered with a 10 micron filter before dynamic light scattering measurements. Purification of the colloids involved centrifugation at 14,000 rpm for 10 minutes, followed by decantation of the supernatent acetonitrile. The colloids were resuspended in acetonitrile through 5 min. of ultrasonication. The methoxy-functionalized COFs were synthesized using the same general procedure by substituting terephthaldehyde with 85.4 mg of 2,5-dimethoxyterephthalaldehyde (Fig. S2).

COF functionalization. The COF shell was functionalized by tethering the aldehyde functionalized BAr^F compound to unreacted amines at the COF surface. 50 mg of 3-(3-(4-formylphenoxy) propyl)-1-methyl-1H-imidazol-3-ium BAr^F and 50 mg of purified colloidal COF were dissolved/suspended in acetonitrile and reacted at 90°C for 24 h. The functionalized COF was purified with repeated centrifugation in acetonitrile to ensure all unreacted BAr^F salt was removed. FTIR was used to confirm successful funtionalization by identifying C-F and imidazolium stretches at 1150 cm^{-1} and 680 cm^{-1}, respectively, that were not present in the parent COF (Fig. S21).

Porous liquid synthesis. Porous liquids were synthesized by mixing the colloidal COF suspension in acteonitrile with the BAr^F ionic liquid. Following 5 min. of ultrasonication, acetonitrile was removed with a rotary evaporator. The porous liquids were dried under vacuum on a Schlenk line at 100 mtorr at 90°C for 48 h.

4.2. Instrumentation

Dynamic light scattering (DLS). Particle size distributions were measured with a Malvern Panalytical Zetasizer Nano series in acetonitrile in a glass cuvette. Three consecutive measurements were performed for each sample to confirm aggregation was not occurring on the timescale of the measurement.

X-Ray Diffraction (XRD). XRD measurments were performed on a PANalytical PW3040 X-Ray Diffractometer using Cu Kα (λ = 1.54 Å) radiation. The scan rate was 2°/min, with a current of 40 mA and a voltage of 45 kV.

Nuclear Magnetic Resonance (NMR). ^{1}H NMR (400 MHz) and ^{13}C NMR (100 MHz) were recorded on a Bruker Avance III HD NanoBay NMR spectrometer. Residual solvent peaks were used as the internal standards for ^{1}H and ^{13}C NMR spectra. The ^{19}F MAS NMR experiments were performed at the Environmental Molecular Sciences Laboratory (EMSL) on an Agilent 850 WB with a direct drive (VNMRS) NMR console. The samples (~50 mg) were packed into 4 mm zirconia rotors with vespel spacers. The NMR probe utilized was an Agilent 4 mm HFXY MAS probe tuned in HFC mode, and the MAS frequency was 10 kHz. The ^{19}F NMR spectra were obtained at 0 °C and with a static magnetic field strength of 20.0 T (Larmor frequencies of 849.727 MHz and 799.457 MHz for ^{1}H and ^{19}F irradiation, respectively). The $\pi/2$ pulse used was 4.75 μs, for 64 transients with a recycle delay of 5 s.

Diffuse Reflectance Infrared Fourier Transform Spectroscopy (DRIFTS). DRIFTS measurements were performed using a Thermo Scientific Nicolet 6700 with a liquid N_2 cooled HgCdTe detector and Harrick Scientific Praying Mantis Diffuse Reflection Accessory. The samples were prepared as 10 wt.% mixtures in a KBr matrix. Background measurements were collected in air at room temperature.

Physisorption measurements. Isotherms were collected on a Micromeritics ASAP 2020. Each sample was degassed at 170°C prior to analysis and transferred to the physisorption instrument without air exposure. N_2 isotherms were collected for the solid-state materials at 77K with a 10 second equilibration time. CO_2 isotherms were collected at 0°C. The equilibration time was 30 seconds for solid-state COFs and 10 minutes for the porous liquids, the latter to account for slow diffusion of gas through the viscous ionic liquid. The Brunauer-Emmet-Teller (BET) method was used to determine the surface area. A DFT slit-pore model was used to extract pore size distributions.

Temperature programmed desorption (TPD). TPD measurements were performed on a calibrated, custom built system equipped with a Stanford Research Systems RGA 100, capable of measuring m/z = 1-100 amu. M/z range of 1-50 amu was used for the CO_2 and CH_4 measurements. Each sample was degassed at 170°C prior to analysis and was not exposed to air. The samples were heated at a ramp rate of 15°C/minute. A type K thermocouple was used to monitor the temperature. Between 5-10 mg of active COF material was used for a given measurement. The samples were loaded directly into a quartz tube connected to the TPD system, as described by Hurst, *et al.*[56] The sample was dosed with gas at 70°C. The solid-state samples were dosed for 10 min. (longer dose times did not increase gas uptake). The liquid samples were dosed for 1 h to account for slow diffusion through the viscous materials. The sample was then quenched with a dry ice and ethanol bath (-78°C) for the CO_2 measurements, and a liquid N_2 and ethanol bath (-115°C) for CH_4 measurements. While the sample was frozen, the head space was evacuated. Experimental parameters were controlled via a LabView interface that is connected to the RGA, heating system, and pressure gauges. The output signal from the mass spectrometer was divided by the total sample mass to get a normalized signal. The normalized signal was integrated over the temperature range of interest to determine total gas uptake. The baseline pressure before heating was approximately 10^{-8} Torr.

Conflicts of interest

There are no conflicts to declare.

Acknowledgements

This work was authored in part by Alliance for Sustainable Energy, LLC, the manager and operator of the National Renewable Energy Laboratory for the U.S. Department of Energy (DOE) under Contract No. DE-AC36-08GO28308. Funding provided by the Hydrogen Materials Advanced Research Consortium (HyMARC), established as part of the Energy Materials Network under the U.S. Department of Energy, Office of Energy Efficiency and Renewable Energy, Fuel Cell Technologies Office. The views expressed in the article do not necessarily represent the views of the DOE or the U.S. Government. The U.S. Government retains and the publisher, by accepting the article for publication, acknowledges that the U.S. Government retains a nonexclusive, paid-up, irrevocable, worldwide license to publish or reproduce the published form of this work, or allow others to do so, for U.S. Government purposes.

Notes and references

1 N. O'Reilly, N. Giri and S. L. James, *Chem. - Eur. J.*, 2007, **13**, 3020–3025.

2 J. Zhang, S.-H. Chai, Z.-A. Qiao, S. M. Mahurin, J. Chen, Y. Fang, S. Wan, K. Nelson, P. Zhang and S. Dai, *Angew. Chem., Int. Ed.*, 2015, **54**, 932–936.

3 N. Giri, M. G. Del Pópolo, G. Melaugh, R. L. Greenaway, K. Rätzke, T. Koschine, L. Pison, M. F. C. Gomes, A. I. Cooper and S. L. James, *Nature*, 2015, **527**, 216–220.

4 K. Jie, N. Onishi, J. A. Schott, I. Popovs, D.-e. Jiang, S. Mahurin and S. Dai, *Angewandte Chemie International Edition*, 2020, **59**, 2268–2272.

5 J. Cahir, M. Y. Tsang, B. Lai, D. Hughes, M. A. Alam, J. Jacquemin, D. Rooney and S. L. James, *Chem. Sci.*, 2020, **11**, 2077–2084.

6 S. He, L. Chen, J. Cui, B. Yuan, H. Wang, F. Wang, Y. Yu, Y. Lee and T. Li, *J. Am. Chem. Soc.*, 2019, **141**, 19708–19714.

7 P. Li, H. Chen, J. A. Schott, B. Li, Y. Zheng, S. M. Mahurin, D.-e. Jiang, G. Cui, X. Hu, Y. Wang *et al.*, *Nanoscale*, 2019, **11**, 1515–1519.

8 M. Costa Gomes, L. Pison, C. Červinka and A. Padua, *Angew. Chem., Int. Ed.*, 2018, **130**, 12085–12088.

9 S. Liu, J. Liu, X. Hou, T. Xu, J. Tong, J. Zhang, B. Ye and B. Liu, *Langmuir*, 2018, **34**, 3654–3660.

10 A. J. Howarth, A. W. Peters, N. A. Vermeulen, T. C. Wang, J. T. Hupp and O. K. Farha, *Chem. Mater.*, 2017, **29**, 26–39.

11 M. Hasib-ur Rahman, M. Siaj and F. Larachi, *Chem. Eng. Process.*, 2010, **49**, 313–322.

12 Y. Chen, F. Mutelet and J.-N. Jaubert, *Fluid Phase Equilib.*, 2014, **372**, 26–33.

13 P. J. Waller, F. Gándara and O. M. Yaghi, *Acc. Chem. Res.*, 2015, **48**, 3053–3063.

14 X. Feng, X. Ding and D. Jiang, *Chem. Soc. Rev.*, 2012, **41**, 6010–6022.

15 S. S. Han, H. Furukawa, O. M. Yaghi and W. A. Goddard Iii, *J. Am. Chem. Soc.*, 2008, **130**, 11580–11581.

16 H. Furukawa and O. M. Yaghi, *J. Am. Chem. Soc.*, 2009, **131**, 8875–8883.

17 W. A. Braunecker, S. Shulda, M. B. Martinez, K. E. Hurst, J. T. Koubek, S. Zaccarine, R. E. Mow, S. Pylypenko, A. Sellinger, T. Gennett and J. C. Johnson, *ACS Mater. Lett.*, 2020, **2**, 227–232.

18 Q. Fang, J. Wang, S. Gu, R. B. Kaspar, Z. Zhuang, J. Zheng, H. Guo, S. Qiu and Y. Yan, *J. Am. Chem. Soc.*, 2015, **137**, 8352–8355.

19 L. Bai, S. Z. F. Phua, W. Q. Lim, A. Jana, Z. Luo, H. P. Tham, L. Zhao, Q. Gao and Y. Zhao, *Chem. Commun.*, 2016, **52**, 4128–4131.

20 G. Zhang, X. Li, Q. Liao, Y. Liu, K. Xi, W. Huang and X. Jia, *Nat. Comm.*, 2018, **9**, 1–11.

21 B. K. Hughes, W. A. Braunecker, D. C. Bobela, S. U. Nanayakkara, O. G. Reid and J. C. Johnson, *J. Phys. Chem. Lett.*, 2016, **7**, 3660–3665.

22 Q. Fang, S. Gu, J. Zheng, Z. Zhuang, S. Qiu and Y. Yan, *Angew. Chem., Int. Ed.*, 2014, **53**, 2878–2882.

23 S. Lin, C. S. Diercks, Y.-B. Zhang, N. Kornienko, E. M. Nichols, Y. Zhao, A. R. Paris, D. Kim, P. Yang, O. M. Yaghi *et al.*, *Science*, 2015, **349**, 1208–1213.

24 H. Xu, J. Gao and D. Jiang, *Nat. Chem.*, 2015, **7**, 905.

25 T. Banerjee, F. Haase, G. Savasci, K. Gottschling, C. Ochsenfeld and B. V. Lotsch, *J. Am. Chem. Soc.*, 2017, **139**, 16228–16234.

26 Y. Ma, Y. Wang, H. Li, X. Guan, B. Li, M. Xue, Y. Yan, V. Valtchev, S. Qiu and Q. Fang, *Angew. Chem. Int. Ed.*, 2020, doi:10.1002/anie.202005277.

27 P. Horcajada, C. Serre, D. Grosso, C. Boissiere, S. Perruchas, C. Sanchez and G. Férey, *Adv. Mat.*, 2009, **21**, 1931–1935.

28 Y. Peng, Y. Li, Y. Ban, H. Jin, W. Jiao, X. Liu and W. Yang, *Science*, 2014, **346**, 1356–1359.

29 G. Zheng, S. de Marchi, V. López-Puente, K. Sentosun, L. Polavarapu, I. Pérez-Juste, E. H. Hill, S. Bals, L. M. Liz-Marzán, I. Pastoriza-Santos *et al.*, *Small*, 2016, **12**, 3935–3943.

30 P. Wang, J. Zhao, X. Li, Y. Yang, Q. Yang and C. Li, *Chem. Commun.*, 2013, **49**, 3330–3332.

31 J. Zhuang, C.-H. Kuo, L.-Y. Chou, D.-Y. Liu, E. Weerapana and C.-K. Tsung, *ACS nano*, 2014, **8**, 2812–2819.

32 G. Lu, C. Cui, W. Zhang, Y. Liu and F. Huo, *Chem.: Asian J*, 2013, **8**, 69–72.

33 Z. Ou, X. Song, W. Huang, X. Jiang, S. Qu, Q. Wang, P. V. Braun, J. S. Moore, X. Li and Q. Chen, *ACS Appl. Mater. Interfaces*, 2018, **10**, 40990–40995.

34 J. Troyano, A. Carné-Sánchez, C. Avci, I. Imaz and D. Maspoch, *Chem. Soc. Rev.*, 2019, **48**, 5534–5546.

35 M. Sindoro, N. Yanai, A.-Y. Jee and S. Granick, *Acc. Chem. Res.*, 2014, **47**, 459–469.

36 B. J. Smith, L. R. Parent, A. C. Overholts, P. A. Beaucage, R. P. Bisbey, A. D. Chavez, N. Hwang, C. Park, A. M. Evans, N. C. Gianneschi *et al.*, *ACS Cent. Sci.*, 2017, **3**, 58–65.

37 R. L. Li, N. C. Flanders, A. M. Evans, W. Ji, I. Castano, L. X. Chen, N. C. Gianneschi and W. R. Dichtel, *Chem. Sci.*, 2019, **10**, 3796–3801.

38 Y. Zhao, L. Guo, F. Gándara, Y. Ma, Z. Liu, C. Zhu, H. Lyu, C. A. Trickett, E. A. Kapustin, O. Terasaki *et al.*, *J. Am. Chem. Soc.*, 2017, **139**, 13166–13172.

39 H. S. Sasmal, A. Halder, S. Kunjattu H, K. Dey, A. Nadol, T. G. Ajithkumar, P. Ravindra Bedadur and R. Banerjee, *J. Am. Chem. Soc.*, 2019, **141**, 20371–20379.

40 A. M. Evans, L. R. Parent, N. C. Flanders, R. P. Bisbey, E. Vitaku, M. S. Kirschner, R. D. Schaller, L. X. Chen, N. C. Gianneschi and W. R. Dichtel, *Science*, 2018, **361**, 52–57.

41 A. M. Evans, I. Castano, A. Brumberg, L. R. Parent, A. R. Corcos, R. L. Li, N. C. Flanders, D. J. Gosztola, N. C. Gianneschi, R. D. Schaller *et al.*, *J. Am. Chem. Soc.*, 2019, **141**, 19728–19735.

42 D. Rodríguez-San-Miguel, A. Yazdi, V. Guillerm, J. Pérez-Carvajal, V. Puntes, D. Maspoch and F. Zamora, *Chem. - Eur. J.*, 2017, **23**, 8623–8627.

43 W. Ma, Q. Zheng, Y. He, G. Li, W. Guo, Z. Lin and L. Zhang, *J. Am. Chem. Soc.*, 2019, **141**, 18271–18277.

44 K. Geng, T. He, R. Liu, S. Dalapati, Z. L. Ke Tian Tan, S. Tao, Y. Gong, Q. Jiang and D. Jiang, *Chem. Rev.*, 2020, **120**, 8814–8933.

45 H. Li, D. Jiehua, X. Guan, F. Chen, C. Li, L. Zhu, M. Xue, Y. Yan, V. Valtchev, S. Qiu and Q. Fang, *ChemRxiv Preprint*, 2020, https://doi.org/10.26434/chemrxiv.12479075.v1.

46 F. J. Uribe-Romo, J. R. Hunt, H. Furukawa, C. Klock, M. O'Keeffe and O. M. Yaghi, *J. Am. Chem. Soc.*, 2009, **131**, 4570–4571.

47 D. M. Fischbach, G. Rhoades, C. Espy, F. Goldberg and B. J. Smith, *Chem. Commun.*, 2019, **55**, 3594–3597.

48 M. Kaliner and T. Strassner, *Tetrahedron Lett.*, 2016, **57**, 3453–3456.

49 W. Shan, P. F. Fulvio, L. Kong, J. A. Schott, C.-L. Do-Thanh, T. Tian, X. Hu, S. M. Mahurin, H. Xing and S. Dai, *ACS Appl. Mater. Interfaces*, 2018, **10**, 32–36.

50 M. Waechtler, M. Sellin, A. Stark, D. Akcakayiran, G. Findenegg, A. Gruenberg, H. Breitzked and G. Buntkowsky, *Phys. Chem. Chem. Phys.*, 2010, **12**, 11371–11379.

51 S. L. Grage, U. H. Dürr, S. Afonin, P. K. Mikhailiuk, I. V. Komarov and A. S. Ulrich, *J. Magn. Reson.*, 2008, **191**, 16–23.

52 S. L. Grage and A. S. Ulrich, *J. Magn. Reson.*, 2000, **146**, 81–88.

53 E. B. Brouwer, R. Challoner and R. K. Harris, *Solid State Nucl. Magn. Reson.*, 2000, **18**, 37–52.

54 M. K. Muthayala and A. Kumar, *ACS Comb. Sci.*, 2012, **14**, 5–9.

55 S. Kandambeth, V. Venkatesh, D. B. Shinde, S. Kumari, A. Halder, S. Verma and R. Banerjee, *Nature Commun.*, 2015, **6**, 6786.

56 K. Hurst, M. Heben, J. Blackburn, T. Gennett, A. Dillon and P. Parilla, *Rev. Sci. Instrum.*, 2013, **84**, 025103.

For Table of Contents Only

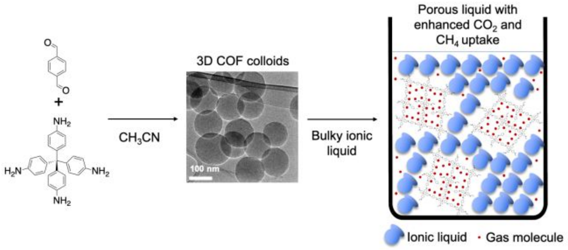

Colloidal COFs suspended in a bulky, size-excluded ionic liquid create a ‘porous liquid’ with enhanced gas uptake.